Anal. Chem. **2003,** *75,* 4975−4982

Temperature-Induced Apparent Mass Changes Observed during Quartz Crystal Microbalance Measurements of Atomic Layer Deposition

M. N. Rocklein[†] and S. M. George*[,†,‡]

Department of Chemistry and Biochemistry, and Department of Chemical Engineering, University of Colorado, Boulder, Colorado 80309-0215

The quartz crystal microbalance (QCM) is a valuable in situ probe of surface chemistry and film growth during atomic layer deposition (ALD). Unfortunately, the QCM is sensitive to both mass and temperature effects that complicate the interpretation of QCM measurements. To characterize the temperature effects, QCM measurements are performed at 170 °C in a hot-wall, ALD flow reactor using pulses of inert and other unreactive probe gases that simulate reactant dosing during ALD. The difference between the probe gas temperature and the QCM sensor temperature is shown to cause instantaneous positive or negative apparent mass transients during the gas pulse. In addition, there is a net apparent mass drift after the gas pulse. The apparent mass transients and apparent mass drifting can lead to misinterpretation of ALD surface chemistry and produce error in measured ALD growth rates. Temperature-induced apparent mass changes are shown to be affected by the temperature profile in the ALD flow reactor before the QCM sensor. Changes in the gas flux during the ALD dosing sequence, changes in the type of dosing gas, and adiabatic cooling of the dosing gas can also produce temperature-induced apparent mass changes. The temperature effects on the QCM sensor are also demonstrated during Al_2O_3 ALD growth using $Al(CH_3)_3$ and H_2O. Experimental methods using unreactive probe gases, such as SF_6, are developed to tune the temperature profile of the ALD flow reactor to minimize the temperature-induced apparent mass changes.

The quartz crystal microbalance (QCM) is a useful tool for quantifying mass deposition resulting from thin-film growth. For atomic layer deposition (ALD), the QCM is extremely useful for probing the ALD surface reactions because of its submonolayer resolution and rapid time response.[1] If the temperature of the quartz crystal is constant during the ALD reactions, then the detected change of mass per time is accurate. If the temperature fluctuates, real mass changes versus time are measured concurrent with the apparent mass changes caused by the temperature dependence of the quartz crystal. Consequently, the temperature-dependent apparent mass changes must be characterized and minimized to allow the QCM to provide an accurate monitoring of ALD reactions and ALD growth.

In quartz crystal resonators, the change of frequency (f) responds to a change in temperature ($T - T_o$) according to[2,3]

$$\Delta f = (f - f_o) = a_1 f_o(T - T_o) + a_2 f_o(T - T_o)^2 + a_3 f_o(T - T_o)^3 + \ldots \quad (1)$$

f_o is the frequency at T_o, T_o is any reference temperature, and a_1, a_2, and a_3 are empirically determined constants related to the crystal orientation.[4] For the commonly employed AT-type quartz resonators, eq 1 is cubic and dominated by the a_1 and a_3 values.[5] Consequently, the first derivative (df/dT) provides a frequency−temperature dependence that is essentially quadratic with respect to temperature. The local minimum is centered near room temperature and is typically negative in value. This produces two "crossover" temperatures that display zero frequency−temperature dependence. Typical AT-type resonators have a relatively small frequency−temperature dependence over a large temperature range between −45 and 90 °C. For an angle of crystal cut near $\theta = 35°20'$, the error is $\leq \pm 1$ ppm/°C.[4] At temperatures greater than ∼90 °C, the frequency−temperature dependence is positive and dramatically increases with increasing temperature.

One solution to minimize temperature-dependent effects is to select an appropriate angle of crystal cut for every desired temperature range. A zero frequency−temperature dependence can be extended up to at least 250 °C for AT-type crystals with an angle of crystal cut near $\theta = 37°30'$.[5,6] Unfortunately, a small frequency−temperature dependence of $\leq \pm 0.5$ ppm/°C is expected for a much smaller temperature range estimated to be <20 °C.[4] Instead of quartz, microbalance techniques using gallium phosphate ($GaPO_4$) resonators with an appropriate crystal cut may provide a small frequency−temperature dependence at much

* Corresponding author. Fax: 303-492-5894. E-mail: steven.george@colorado.edu.

[†] Department of Chemistry and Biochemistry.

[‡] Department of Chemical Engineering.

(1) Geissler, D.; Hartig, P.; Wunsche, M.; Meyer, H.; Schumacher, R. *Electroanalysis* **1999**, *11*, 412.

(2) Fairweather, D.; Richards, R. C. *Quartz Crystals as Oscillators and Resonators*; Marconi's Wireless Telegraph Co.: Chelmsford, England, 1957.

(3) Frerking, M. E. *Crystal Oscillator Design and Temperature Compensation*; Van Nostrand Reinhold Co.: New York, 1978.

(4) Bechmann, R. *Proc. IRE* **1956**, *44*, 1600.

(5) Bechmann, R. *Proc. IRE* **1960**, 1494.

(6) Phelps, F. P. *Proc. Eleventh Annual Symposium on Frequency Control*; Asbury Park, NJ, May 7−9, 1957; pp 256−276.

10.1021/ac030141u CCC: $25.00
Published on Web 08/23/2003

higher temperatures up to 970 °C.[7] Another solution to reducing temperature effects is to compensate for drift using analog or digital voltage compensation.[3] The temperature dependence can be determined in the absence of any real mass changes, and then this temperature dependence is used to distinguish real mass changes.

The relationship between the change of resonant frequency (f) and the change in mass (Δm) is linear and negative:[8,9]

$$\Delta f = -C\Delta m \quad (2)$$

C is a crystal-dependent sensitivity factor that includes the fundamental resonant frequency (f_0), the surface area (A), the density (ρ) and the shear modulus (μ):

$$C = 2f_0^2/(A(\mu\rho)^{0.5}) \quad (3)$$

Equations 1 and 2 can be equated to yield the temperature-induced apparent mass change:

$$-\Delta m = -(m - m_o) = C_1(T - T_o) + C_2(T - T_o)^2 + C_3(T - T_o)^3 \quad (4)$$

where C_1, C_2, and C_3 equal $a_1\ f_o/C$, $a_2\ f_o/C$, and $a_3\ f_o/C$, respectively. If C_1, C_2, and C_3 can be determined in the absence of real mass changes, then these values can be used to remove the effects of temperature during mass deposition. To determine the temperature dependence, the temperature of the crystal sensor must be monitored accurately without significant noise or spatial and temporal hysteresis. Thermal conditioning of the crystal may also improve the reproducibility of the temperature-induced apparent mass change.[10]

Another possibility is to use an additional reference crystal[8,11−13] that is protected from mass changes yet experiences temperature changes identical to the measurement crystal. Subtraction of the reference crystal value from the measurement crystal value then removes the temperature effect. However, this "dual crystal method" is difficult to employ for gas-phase processes. Many temperature effects are caused by transient gas effects that the reference crystal may not detect. Another recently reported method uses baseline subtraction.[14] This method assumes that any QCM drift can be modeled with a polynomial by using QCM data before and after the growth period. Unfortunately, instantaneous apparent mass changes and apparent mass drift due to transient gas effects cannot be compensated by baseline subtraction methods.

This paper demonstrates experimental methods to both identify and minimize temperature-induced apparent mass changes during QCM measurements. Temperature transients caused by gas pulsing can be controlled by modifying the temperature profile along the length of the reactor tube before the QCM. The temperature of the transient gas is shown to dictate the magnitude and sign of the instantaneous apparent mass changes. Consequently, the temperature profile along the length of the reactor can be tuned to minimize temperature-induced apparent mass transients. In addition, positive or negative apparent mass transients generally lead to positive or negative mass drifting during the repeated ALD pulsing sequence. The amount of mass drift can be minimized by reducing the magnitude of the apparent mass transients.

The temperature-induced apparent mass transients observed during gas pulsing are demonstrated with a variety of inert and other unreactive probe gases and during Al_2O_3 ALD. The magnitude and sign of the temperature change caused by the transient gas pulses produce error in the measured growth rates. Additionally, adiabatic cooling of expanding reactant gases can cause significant temperature transients that lead to apparent mass transients during ALD growth. This paper characterizes the possible temperature effects during QCM measurements of ALD. Based on these investigations, a number of recommendations are proposed to minimize these temperature effects for more reliable QCM studies.

EXPERIMENTAL SECTION

QCM measurements were conducted using a commercial Maxtek TM-400 QCM system and recorded on a personal computer at ∼10 Hz. Frequency and mass resolution at 6.0 MHz are 0.03 Hz and 0.375 ng/cm^2, respectively. From eq 2, the QCM sensitivity factor is $C = -0.08$ Hz/(ng/cm^2) at 6.0 MHz. Polished AT-type crystals were obtained from Colorado Crystal Corp. The quartz crystals were plano-convex, 0.550-in. diameter and operated at 6-MHz nominal frequency in the fundamental mode. These sensors contained an Inficon electrode pattern on the protected convex surface. ALD growth occurs on the top planar electrode previously polished using ∼0.3 μm-diameter cerium oxide powder. The sensor crystal is held by a Maxtek Next Generation Cool Drawer that inserts into a stainless steel housing (Maxtek BSH-150 bakeable single sensor head feedthrough) that was originally designed for water-cooling.

To prevent mass deposition on the back of the crystal, both the insert drawer and front crystal electrode edge are sealed to the crystal housing using an electrically conducting epoxy (Epotek P1011, Epoxy Technologies). This epoxy has a thermal conductivity of 1.3 W m^{-1} K^{-1} and is stable for continuous operation up to 350 °C. Additionally, the water-cooling tubes have been modified to provide an independent N_2 purge estimated at 15 sccm on the back of the crystal.[15] The QCM temperature is monitored with a shielded type K thermocouple probe inserted into the underside of the stainless steel housing and attached with epoxy.[15] The temperature of the quartz crystal is expected to respond more rapidly to changes in the carrier gas temperature than the stainless steel housing and thermocouple probe.

(7) Thanner, H.; Krempl, P. W.; Wallnofer, W.; Worsch, P. M. *Vacuum* **2002**, *67*, 687.
(8) Dunham, G. C.; Benson, N. H.; Petelenz, D.; Janata, J. *Anal. Chem.* **1995**, *67*, 267.
(9) Sauerbrey, G. *Z. Phys.* **1959**, *155*, 206.
(10) Narine, S. S.; Slavin, A. J. *J. Vac. Sci. Technol. A* **1998**, *16*, 1857.
(11) Bruckenstein, S.; Michalski, M.; Fensore, A.; Li, Z.; Hillman, A. R. *Anal. Chem.* **1994**, *66*, 1847.
(12) Mecea, V. M.; Carlsson, J. O.; Heszler, P.; Bartan, M. *Vacuum* **1995**, *46*, 691.
(13) Langer, A.; Patton, J. T. *Vac. Microbalance Technol.* **1966**, *5*, 231.
(14) Rahtu, A.; Ritala, M. *Appl. Phys. Lett.* **2002**, *80*, 521.
(15) Elam, J. W.; Groner, M. D.; George, S. M. *Rev. Sci. Instrum.* **2002**, *73*, 2981.

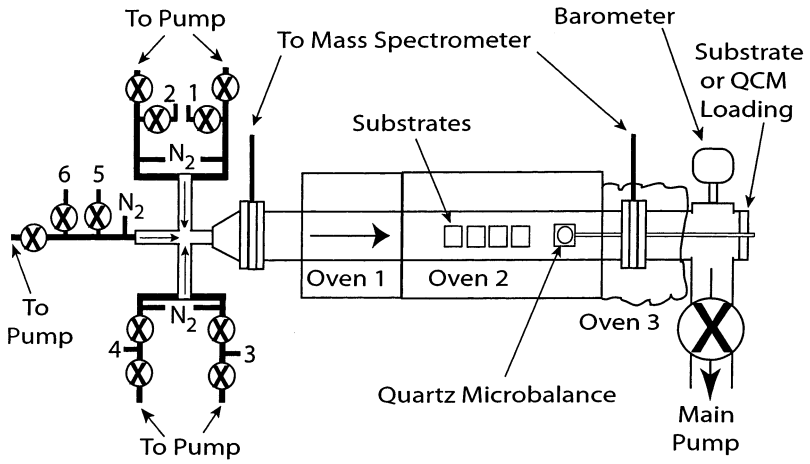

Figure 1. Schematic representation of the gas delivery lines and flow tube ALD reactor.

Reactant and carrier gas flow is parallel to the crystal surface. Gases or vapors used in this study were N_2 (ultrahigh purity, Airgas Intermountain, Inc.), He (Airgas Intermountain, Inc.), CO_2 (Mattheson Gas Products, Inc.), Xe (Cryogenic Rare Gases Lab. Inc.), SF_6 (Scott Specialty Gases, Inc.), $Al(CH_3)_3$ (Aldrich Chemical Co., Inc.), and H_2O (Optima, Fisher Scientific). Thirteen type K thermocouples are attached along the length of the reactor tube using an electrically insulating ceramic glue (Ceramabond 685, Aremco Products, Inc.).

Figure 1 shows a schematic of the hot-wall, low-pressure, viscous-flow reactor and the reactant dosing lines. The forelines are made from stainless steel VCR connections. The main reactor is a stainless steel tube with a 1.5-in outer diameter connected to the forelines using a conical reducer with Conflat flanges and copper gaskets. Up to six different reactants from six channels may be pulsed into various N_2 gas carrier streams in an automated pulsed-valve sequence. The pulsed valves are diaphragm-sealed and pneumatically operated (Fujikin, Inc. or Swagelok, Inc.). The total N_2 flow of ~280 sccm is controlled by three mass-flow controllers (MKS Instruments) and produces a chamber pressure of ~1.6 Torr. The total chamber pressure is measured using a 0.001−10 Torr capacitance manometer maintained near 30 °C.

To reduce the residence time of the reactant gases or vapors, the forelines are heated to 50−80 °C using a voltage regulator, heating tape, and aluminum foil insulation. Ovens 1 and 2 are 6- and 12-in. ceramic-insulated heaters (Watlow), respectively, with independent temperature settings, proportional−integral−derivative (PID) control, and automated tuning. Oven 1 provides preheating to the carrier gas stream while oven 2 provides a temperature plateau for samples in the tube and the QCM sensor. Oven 3 is constructed of multiple layers of electric heating tape and aluminum foil and is under PID control from a personal computer and a 40-V, 25-A dc power supply. The QCM temperature is passively controlled, primarily by oven 2 and secondly by oven 3.

Figure 2 is included to provide a visual understanding of the gas exposure process for channel 1. Channel 2 operates in a similar manner with a shared reagent pump and a shared N_2 mass-flow controller. The reagent gas or vapor resides behind the closed pulsed valve at a pressure controlled by a gas regulator or by its temperature-dependent vapor pressure. In this "off" state, the

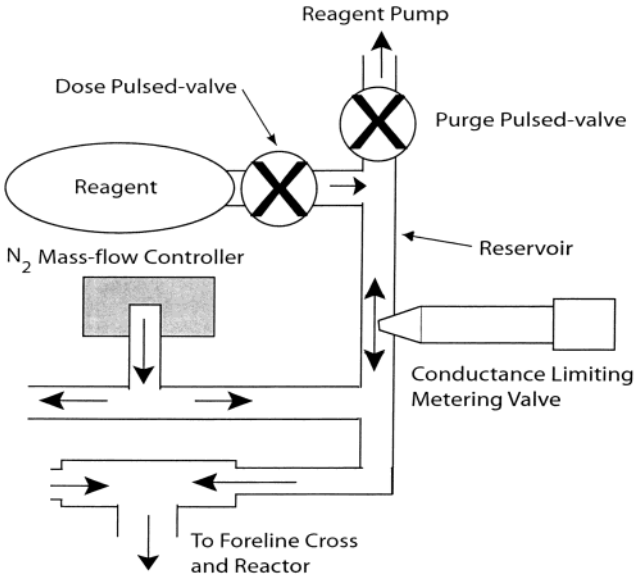

Figure 2. Enlargement of channel 1 of the gas delivery line that illustrates the introduction of the gas pulses into the ALD reactor.

purge pulsed valve is open to the reactant pump allowing a small portion of the N_2 carrier gas to flow through the conductance-limiting metering valve and flush the reservoir region. The majority of the N_2 carrier gas flows to the main cross and then to the reactor and main pump.

When reagent exposure is initiated, the purge pulsed valve closes and the dose pulsed valve opens, allowing the reservoir to fill with reagent gas. In the "on" state, the reagent gas will flow directly into the N_2 stream and be carried to the reactor. The conductance-limiting valve is necessary for higher vapor pressure gases to reduce exposures since the minimum reproducible on−off switching is typically between 40 and 200 ms. Additionally, the conductance-limiting valve prevents some liquid reagents (e.g., H_2O) from boiling due to the low reactor pressures and thereby prevents foreline contamination.

The reagent exposure event is ended by closing the dose pulsed valve and reopening the purge pulsed valve. The quantity of reagent entering the carrier stream is primarily controlled by the reagent backing pressure relative to the reactor pressure, the

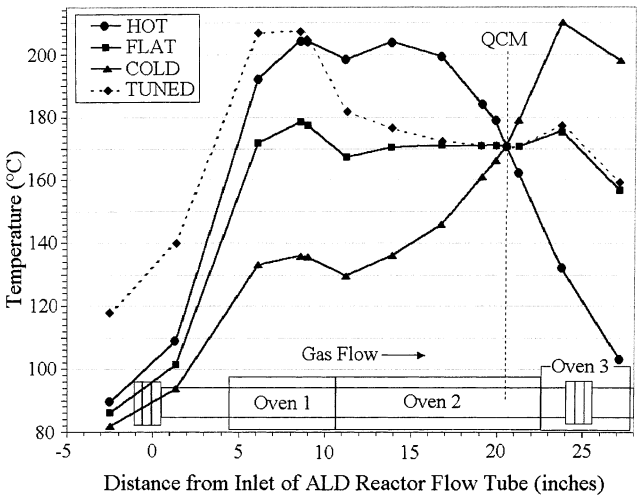

Figure 3. External temperature readings along the length of the flow tube ALD reactor for the HOT, FLAT, COLD, and TUNED temperature profiles. The QCM temperature reading is measured on the QCM housing.

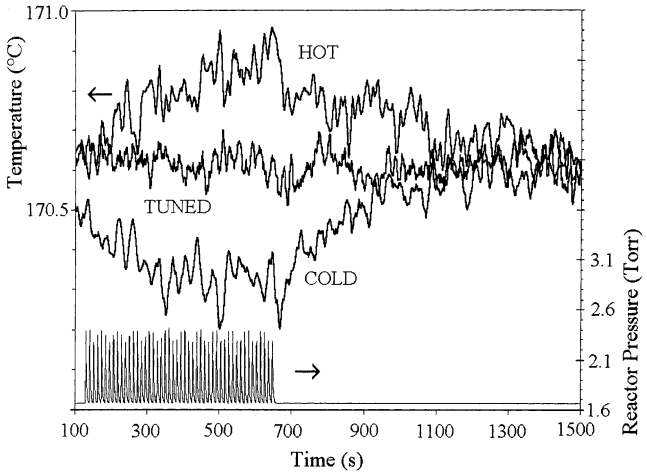

Figure 4. Temperature of the QCM housing during alternating pulses for the probe gas sequence He, CO_2, Xe, and SF_6 for the different reactor temperature profiles. The reactor pressure corresponds to a 1-s gas exposure and a 10-s purge for each probe gas for a total of 12 cycles measured for the COLD temperature profile. Similar gas exposures and reactor pressures were obtained for the HOT and TUNED temperature profiles.

conductance limiting valve setting, and the length of time that the pulsed valves were in the "on" state. Channels 5 and 6 operate in a manner similar to that of channel 1. Channels 5 and 6 share a common purge pulsed valve and a common conductance-limiting valve. Channels 3 and 4 are designed for low-vapor pressure reactants requiring a bubbler operation and were not used in these experiments.

RESULTS AND DISCUSSION

Figure 3 shows four different external temperature profiles along the length of the reactor. These external temperature profiles are created by adjusting the temperature set points of the three ovens and also the reactor forelines. The QCM temperature is measured by an internal thermocouple inserted in the QCM sensor housing. The QCM temperature is kept relatively constant at 170 °C to maintain consistent df/dT and dm/dT values when temperature-induced apparent mass changes are observed.

The HOT profile represents a reactor hotter than the QCM. The FLAT profile represents a relatively flat temperature profile before the QCM. The COLD profile represents a reactor colder than the QCM. The TUNED profile represents a customized temperature profile in which the reactor has a significant preheating zone. Throughout the text, these profiles will be referred to as HOT, FLAT, COLD, and TUNED profiles, respectively. The HOT, FLAT, and COLD profiles are intended to represent common single-oven flow reactors where the QCM is positioned somewhere along a "volcano-shaped" temperature profile.

Figure 4 shows how the internal QCM temperature is affected by introducing a pulse sequence of inert or other unreactive probe gases for the HOT, TUNED, and COLD profiles. The right *Y*-axis is the change in reactor pressure, and the bottom trace is a representative pressure response from the COLD profile for 12 cycles of alternating pulses of He, CO_2, Xe, and SF_6. Each probe gas is pulsed "on" for 1 s followed by 10 s of purging during which a nearly constant background of N_2 carrier gas flows through the reactor. Helium was chosen for its high thermal conductivity and low heat capacity. Xenon was chosen for its low thermal conductivity and low heat capacity. Sulfur hexafluoride was chosen for its moderately low thermal conductivity and very high heat capacity. Carbon dioxide was chosen for its moderate thermal conductivity and moderate heat capacity.

At 400 K and 1 bar (750 Torr), the thermal conductivities[16] in units of mW K^{-1} m^{-1} and heat capacities[16,17] in units of J mol^{-1} K^{-1} for He, CH_4, H_2O, N_2, CO_2, Xe, and SF_6 are (190.6, 20.8), (49.1, 40.6), (27.1, 34.3) (32.3, 29.2), (25.1, 41.3), (7.3, 20.8), and (20.6, 116.4), respectively. Thermal conductivities and heat capacities for most of these probe gases increase with increasing temperature.[16,17] Thermal conductivities are relatively constant above 10−50 Torr and decrease below 10−50 Torr.[18] The thermal conductivity of a mixture of the probe gas and the N_2 carrier gas is approximately a linear function of mole fraction using a "rule of mixtures" formula.[19,20]

The effect of the probe gas pulse sequence on the QCM temperature follows expectations. For the HOT profile, the QCM housing warms during gas dosing and then cools after gas dosing. For the COLD profile, the QCM housing cools during gas dosing and then warms after gas dosing. Gas pulse sequences can create a measurable positive or negative slow temperature drift of the QCM. The sign of this drift depends on the temperature profile of the reactor before the QCM.

Figure 5 shows the apparent mass change measured by the QCM during the pulses of probe gases for the HOT, TUNED, and COLD temperature profiles. The slow mass responses for the HOT profile to lower apparent mass and the COLD profile to higher apparent mass result from the negative dm/dT at 170 °C.

(16) Lide, D. R., Ed. *CRC Handbook of Chemistry and Physics*, 83rd ed.; CRC Press: Boca Raton, FL, 2002; pp 6−175, 175−161, 176−117.
(17) Chase, M. W. *NIST-JANAF Thermochemical Tables*; American Chemical Society: Washington, DC, 1998.
(18) Dushman, S., Lafferty, J. M., EdS. *Scientific Foundations of Vacuum Technique*, 2nd ed.; John Wiley & Sons: New York, 1962.
(19) Bird, R. B.; Stewart, W. E.; Lightfoot, E. N. *Transport Phenomena*; John Wiley & Sons: New York, 1960.
(20) Poling, B. E.; Prausnitz, J. M.; O'Connell, J. P. *The Properties of Gases and Liquids*, 5th ed.; McGraw-Hill: New York, 2001.

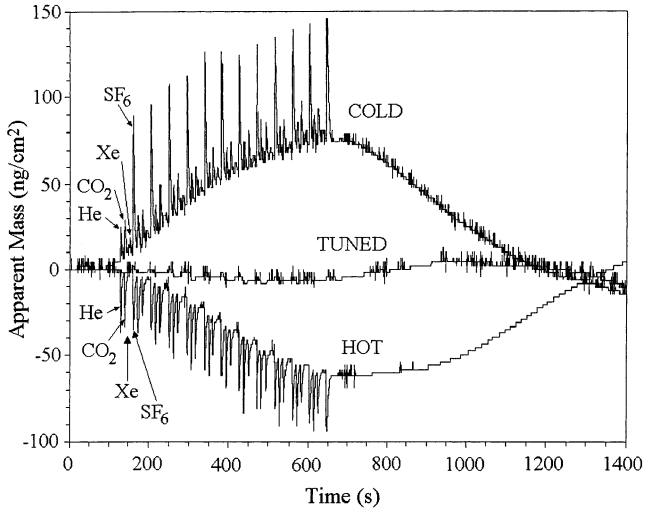

Figure 5. Apparent mass change during 48 probe gas pulses for the COLD, TUNED, and HOT temperature profiles. The probe gas sequence He, CO_2, Xe, and SF_6 corresponds to a 1-s gas exposure and a 10-s purge for each probe gas for a total of 12 cycles.

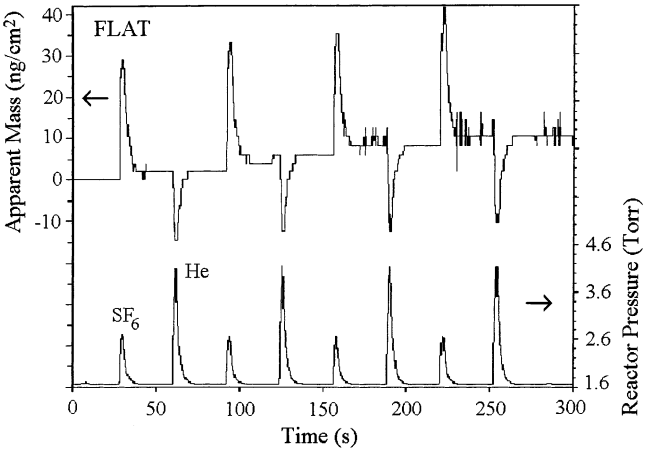

Figure 6. Apparent mass and change in reactor pressure for alternating pulses of SF_6 or He for the FLAT temperature profile.

This behavior clearly shows that a pulse sequence of probe gases can cause positive or negative error in the QCM measurement due to transport of thermal energy.

If the apparent mass drift decreases during the pulse sequence as the QCM approaches a new steady-state temperature, then the absolute error will approach a constant value. The percent error will then decrease with an increasing number of cycles. For example, assume that the mass drift observed from 0 to 700 s corresponding to the COLD or HOT profiles in Figure 5 occurred during 12 cycles of Al_2O_3 ALD. Given an Al_2O_3 ALD growth rate of ~38.5 ng cm^{-2} cycle^{-2} or 1.1 Å/cycle assuming a density of 3.5 g/cm^3, the percent error in the calculated thickness would be +17 or −13%, respectively. For 24 cycles of Al_2O_3 ALD, the percent error in the calculated thickness would be half these values. The decreasing mass drift in Figure 5 indicates that the QCM is slowly approaching a new steady-state temperature. Consequently, these temperature-induced mass changes will cause the most error for growth studies of ultrathin films or for nucleation investigations.

After the exposure sequence, Figure 5 reveals that the mass returns to and then overshoots (above or below) the original starting mass. The maximum mass drift for the COLD profile is ~75 ng/cm^2. Given the induced temperature change shown in Figure 4, this mass drift yields $dm/dT = -280 \pm 80$ ng cm^{-2} °C^{-1} at 170 °C for the COLD profile. The HOT profile yields $dm/dT = -250 \pm 60$ ng cm^{-2} °C^{-1} based on a similar comparison between Figures 4 and 5.

The most remarkable aspect of Figure 5 is the observable fine structure for the HOT and COLD temperature profiles. For the COLD profile, the probe gases are colder than the QCM and appear to cause instantaneous positive apparent mass transients. For the HOT profile, the probe gases are warmer than the QCM and appear to cause instantaneous negative apparent mass transients. Positive or negative mass transients are often observed in QCM measurements during reactant exposure.[14,21−27] Without additional supporting data, QCM mass transients could be either temperature-induced mass transients or real mass changes resulting from adsorption, desorption, or etching processes.

Figure 5 reveals that there are positive or negative apparent mass transients for similar pressure pulses depending on the temperature profile before the QCM. This behavior argues convincingly that the mass transients are caused by temperature effects. In comparison, the curve for the TUNED profile shows very little structure and minimal drift. For both the HOT and COLD temperature profiles in Figure 5, the different probe gases produce mass transients of different magnitudes. However, the inversion of the transients in going from the COLD to HOT profiles for the different probe gases does not scale proportionally. The He and CO_2 mass transients invert and approximately double in magnitude in going from the COLD to HOT profiles. In contrast, the SF_6 mass transients in Figure 5 invert and decrease by ~50% in going from the COLD to HOT profiles.

Figure 6 shows the apparent mass change (left *Y*-axis) and the change in reactor pressure (right *Y*-axis) during several alternating SF_6 and He pulses for the FLAT temperature profile. Positive or negative apparent mass transients can occur dependent on the gas. SF_6 produces a positive mass transient while He produces a negative mass transient caused by QCM sensor cooling and warming, respectively. Presumably, SF_6 cools the QCM sensor because SF_6 never fully equilibrates with the reactor temperatures before the QCM because of its very large heat capacity and lower thermal conductivity. In contrast, He has a small heat capacity and a very high thermal conductivity. Helium responds quickly to the temperature in the flow tube reactor and apparently warms the QCM sensor.

The temperature profile before the QCM was adjusted to minimize the apparent mass transients. The He and SF_6 gas pulses are intentionally large in Figure 6 to accentuate the temperature transients before beginning the tuning procedure. The largest effect in reducing the magnitude of the transients caused by the SF_6 and He pulses was to increase the temperature of oven 1 and

(21) Aarik, J.; Kukli, K.; Aidla, A.; Pung, L. *Appl. Surf. Sci.* **1996**, *103*, 331.
(22) Aarik, J.; Aidla, A.; Uustare, T.; Ritala, M.; Leskela, M. *Appl. Surf. Sci.* **2000**, *161*, 385.
(23) Rahtu, A.; Ritala, M. *Chem. Vap. Deposition* **2002**, *8*, 21.
(24) Rahtu, A.; Ritala, M. *Langmuir* **2002**, *18*, 10046.
(25) Rahtu, A.; Ritala, M. *J. Mater. Chem.* **2002**, *12*, 1484.
(26) Rahtu, A.; Alaranta, T.; Ritala, M. *Langmuir* **2001**, *17*, 6506.
(27) Aarik, J.; Aidla, A.; Jaek, A.; Leskela, M.; Niinisto, L. *J. Mater. Chem.* **1994**, *4*, 1239.

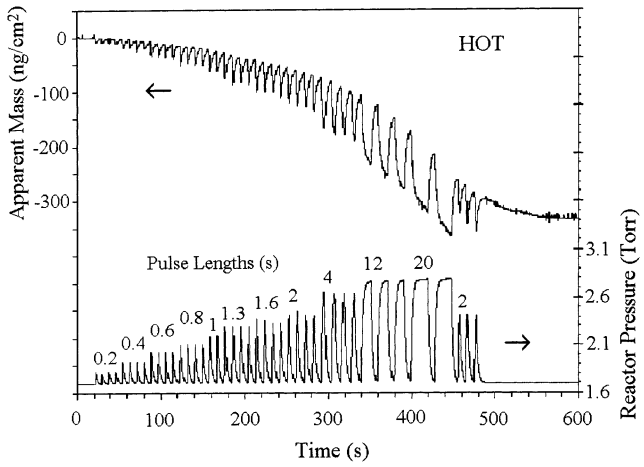

Figure 7. Apparent mass and change in reactor pressure versus time for different SF_6 gas pulses for the HOT temperature profile. The SF_6 pulse lengths from left to right are 0.20, 0.40, 0.60, 0.80, 1.0, 1.3, 1.6, 2.0, 4.0, 12.0, 20.0, and 2.0 s. After each SF_6 gas pulse, the N_2 purge time is 8.0 s. The SF_6 backing pressure is 70 kPa above vacuum.

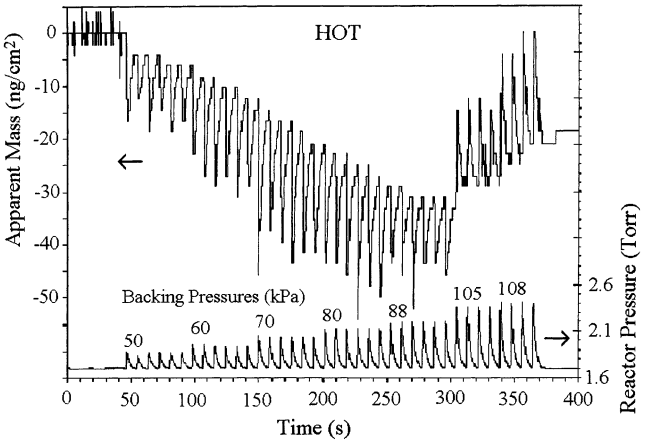

Figure 8. Apparent mass and change in reactor pressure versus time for different SF_6 backing pressures for the HOT temperature profile. The SF_6 backing pressures from left to right are 50, 60, 70, 80, 88, 105, and 108 kPa above vacuum. The SF_6 pulse length is 0.60 s, and the N_2 purge time is 8.0 s.

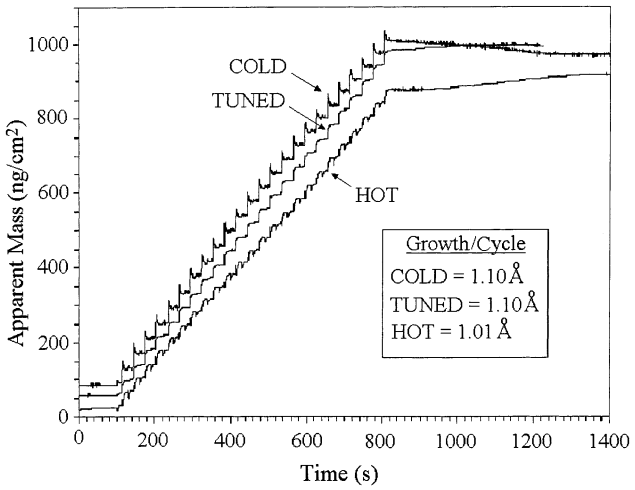

Figure 9. Apparent mass versus time during Al_2O_3 ALD at 170 °C using H_2O and TMA for the COLD, TUNED, and HOT temperature profiles. The alternating exposure sequence for one cycle is as follows: 1-s H_2O pulse; 14-s N_2 purge; 1-s TMA pulse; 14-s N_2 purge. The measurements during 24 cycles for the COLD, TUNED, and HOT temperature profiles are offset for clarity in presentation.

also the reactor forelines. These higher temperatures preheat the SF_6 and apparently reduce the temperature difference between the He and the QCM sensor. Changing the temperature of oven 2 relative to oven 3 causes both mass transient peaks to shift in a common direction with little effect on the peak differences. The tuning procedure to minimize the apparent mass transients eventually produced the TUNED profile shown in Figure 3. Although the FLAT and TUNED external temperature profiles are very similar near the QCM in Figure 3, internal temperature profiles have been modified by the tuning procedure to remove the temperature transients observed in Figure 6 from both the SF_6 and He pulses. The QCM response to the probe gas sequence of He, CO_2, Xe, and SF_6 for the TUNED profile is shown in Figure 5.

The effect of exposure quantity on the QCM signal is observed in Figure 7 for SF_6 gas and the HOT profile. The upper trace is the apparent mass change (left *Y*-axis), and the bottom trace is the change in reactor pressure (right *Y*-axis). For this experiment, the nominal setting for the SF_6 backing pressure is 70 kPa (525 Torr) above vacuum and the pulse length is changed progressively in the following sequence: 0.20, 0.40, 0.60, 0.80, 1.0, 1.3, 1.6, 2.0, 4.0, 12.0, 20.0, and 2.0 s. The observed negative mass transients caused by instantaneous QCM sensor warming increases monotonically with increasing pulse length. Even at the highest pressures corresponding to the longest pulse lengths, the QCM response versus exposure is always negative.

Figure 8 shows results of a similar experiment using the HOT profile. In this experiment, the change in reactor pressure (bottom trace, right *Y*-axis) per pulse was increased by increasing the SF_6 backing pressure incrementally with a constant dose time of 0.6 s. From left to right, the SF_6 backing pressures are as follows: 50, 60, 70, 80, 88, 105, and 108 ± 2 kPa. The upper trace (left *Y*-axis) is the apparent mass change. Increasing the SF_6 backing pressures up to 70 kPa causes an increase in the observed pressure change and a larger negative mass transient. However, the magnitude of the negative mass transient decreases with increasing backing pressure above 80 kPa.

Above 80 kPa, the apparent mass transients eventually invert and grow more positive at higher backing pressures. For these higher backing pressures, the SF_6 gas cools the QCM despite the HOT reactor temperature profile. The most likely explanation is that adiabatic cooling of the probe gas occurs during gas admittance. At higher backing pressures, this adiabatic cooling can have a significant effect on the temperature of the gases reaching the QCM. The inversion behavior was not observed in Figure 7 despite even higher pressure exposures. This behavior is attributed to the lower SF_6 backing pressure of 70 kPa.

Figure 9 shows the QCM signal during 24 cycles of Al_2O_3 ALD using $Al(CH_3)_3$ (TMA) and H_2O[28–30] for the COLD, TUNED, and HOT temperature profiles. These traces have been offset for clarity

(28) Ott, A. W.; Klaus, J. W.; Johnson, J. M.; George, S. M. *Thin Solid Films* **1997**, *292*, 135.
(29) Juppo, M.; Rahtu, A.; Ritala, M.; Leskela, M. *Langmuir* **2000**.
(30) Dillon, A. C.; Ott, A. W.; Way, J. D.; George, S. M. *Surf. Sci.* **1995**, *322*, 230.

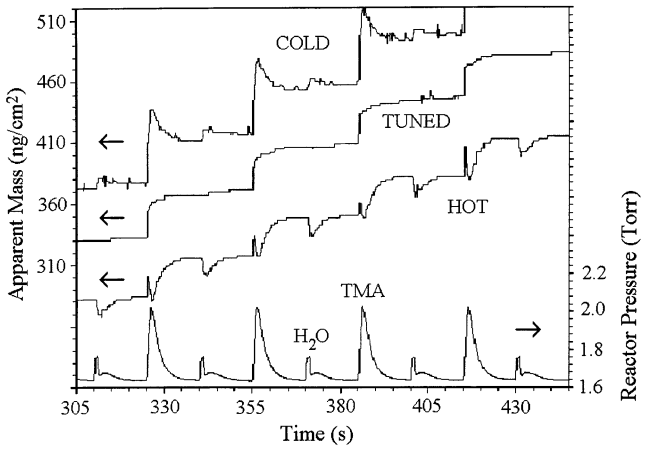

Figure 10. Enlarged view of Figure 9 showing apparent mass versus time during Al_2O_3 ALD at 170 °C for the COLD, TUNED, and HOT temperature profiles. The corresponding change in reactor pressure is also given for the COLD temperature profile.

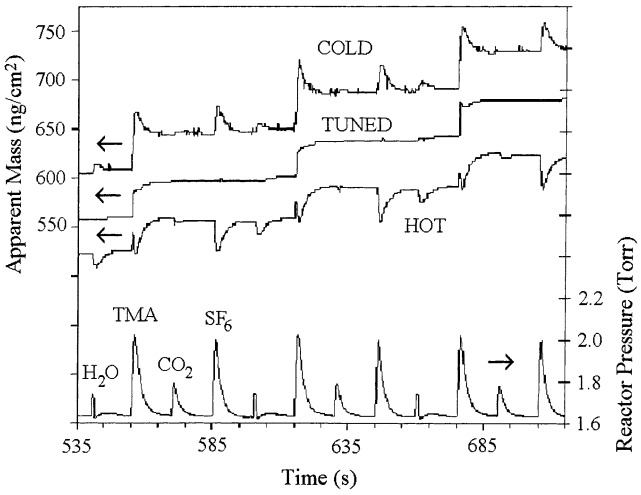

Figure 11. Apparent mass change versus time during Al_2O_3 ALD at 170 °C together with CO_2 and SF_6 probe gas pulses for the COLD, TUNED, and HOT temperature profiles. Each gas exposure is 1 s followed by a 14-s N_2 purge. The three upper traces are offset for clarity in presentation. The corresponding change in reactor pressure is also given for the COLD temperature profile.

in presentation. For each experiment, the initial surface has been prepared similarly by depositing more than 10 Al_2O_3 ALD cycles. The temperature was then allowed to equilibrate for more than 10 min. One Al_2O_3 ALD dosing cycle is as follows: 1 s of H_2O exposure, 14 s of N_2 purge, 1 s of TMA exposure, and 14 s of N_2 purge. The H_2O and TMA exposures are sufficient for saturation of the surface reactions. The N_2 purge times are intentionally longer than necessary to separate the QCM signals resulting from the individual reactant exposures.

Some temperature-induced apparent mass drift is observed during Al_2O_3 ALD growth in Figure 9. The HOT and COLD profiles show slightly nonlinear growth behavior presumably due to QCM temperature changes during growth. After 24 cycles of Al_2O_3 ALD, the subsequent QCM mass drift for the HOT and COLD profiles is $\sim\pm1$ Al_2O_3 ALD cycle QCM mass change. The direction of the mass drift after the 24 cycles of Al_2O_3 ALD follows expectations given a return to the initial thermal conditions. The mass drift that occurs for the TUNED profile after 24 cycles of Al_2O_3 ALD is reduced to $\sim+0.4$ Al_2O_3 ALD cycle QCM mass change. There is somewhat less error for the TUNED profile because the ALD exposure sequence induces less thermal perturbation.

The average Al_2O_3 ALD growth rates may be calculated by dividing the total mass change by the total number of cycles. The QCM mass value at the start of the first cycle was subtracted from the QCM value at the end of the last cycle. The HOT and COLD reactor profiles provide Al_2O_3 ALD growth rates that differ by $\sim$9%. By averaging the subsequent QCM mass values after the last Al_2O_3 ALD cycle as the temperature returns to the initial conditions, the growth rates determined with the HOT and COLD profiles differ in growth rate by $\sim$3%. Consequently, waiting for a length of time following the Al_2O_3 ALD growth will slowly reduce the error caused by the temperature-induced apparent mass drift.

Figure 10 is an enlarged section of Figure 9 showing the QCM measurement during Al_2O_3 ALD for the COLD, TUNED, and HOT profiles. The change in reactor pressure is also shown for the COLD profile. Only the TUNED profile shows a reasonable mass change during the Al_2O_3 ALD surface reactions. During the TMA exposure, the mass increases consistent with the addition of aluminum and methyl groups to the surface according to the reaction

$$AlOH^* + Al(CH_3)_3 \rightarrow AlOAl(CH_3)_2^* + CH_4 \qquad (5)$$

Surface species are designated with an asterisk. The mass change during the H_2O exposure is nearly negligible because OH* species (17 amu) replace CH_3* species (15 amu) according to the reaction

$$AlCH_3^* + H_2O \rightarrow AlOH^* + CH_4 \qquad (6)$$

The COLD and HOT profiles show positive and negative instantaneous apparent mass changes, respectively, superimposed on the real mass changes. Comparisons between the COLD, TUNED, and HOT profiles reveal that the positive and negative apparent mass transients observed during the TMA and H_2O exposures for the COLD and HOT profiles are artifacts. TMA and H_2O are not physically adsorbing and desorbing at 170 °C as might be inferred from the COLD temperature profile. These results illustrate that interpreting the QCM mass step structure during ALD growth is very uncertain. Even for the TUNED profile, there may be slight temperature-induced apparent mass transients that depend on the backing pressure of reactant gas, gas exposure, and gas composition.

Figure 11 shows how probe gases can be incorporated into the reactant exposure sequence to estimate the contribution of the temperature-induced apparent mass change to the observed mass signal. The SF_6 gas introduction conditions were adjusted to minimize the effects of adiabatic cooling. Figure 11 reveals that similar pressure pulses of SF_6 and TMA produce apparent mass transients of similar sign and magnitude for the HOT and COLD temperature profiles. In contrast, no mass transient is observed during SF_6 pressure pulses for the TUNED temperature profile. This behavior indicates that no significant temperature-induced apparent mass transients are affecting the QCM signal during the

TMA exposure for the TUNED profile. The temperature-induced apparent mass transients also appear to be negligible during the H_2O exposure for the TUNED temperature profile.

The temperature profile of the viscous flow reactor can be optimized using the probe gases interspersed with the ALD reactant gases. SF_6 is a good choice because SF_6 has a high heat capacity and a moderate thermal conductivity that should be comparable with various ALD reactant gases. A cold reactor profile before the QCM will cause positive apparent mass transients during SF_6 gas exposure. If adiabatic cooling is minimized, a hot reactor profile before the QCM will cause negative apparent mass transients during SF_6 gas exposure. The optimally tuned reactor profile should produce a negligible mass transient as shown in Figure 11.

Another possible test to evaluate temperature-induced apparent mass transients is to dose the reactant precursor several times. If the surface chemistry of the ALD reaction reaches completion after the first reactant exposure, then the subsequent reactant exposures may reveal apparent mass transients that would be attributed to only temperature perturbations. However, a significant fraction of the reactant may be converted to products during ALD. The product gases may have thermal transport properties different from those of the reactant gases. Consequently, this possible test is not reliable because temperature perturbations may be different for the first reactant exposure and subsequent reactant exposures. Tuning the temperature profile of the viscous flow reactor using probe gases eliminates the complications of surface reactions and changing gas environments.

A number of factors can affect the temperature-induced apparent mass changes observed during QCM measurements. The errors are greater at higher QCM temperatures where df/dT and dm/dT are larger. The errors are also greater for temperature gradients that are larger than the HOT and COLD profiles shown in Figure 3. Larger reactant pulses and shorter purge times also aggravate the QCM error. In addition, the QCM error is worse if the temperature controller is unstable. The errors will also depend on the absolute gas pressure. This investigation has focused on viscous flow conditions where the reactants are entrained in a carrier gas. Errors will be less under molecular flow conditions because of the reduced thermal load on the QCM sensor.

Other factors also affect the reliability of QCM measurements. The external oscillator component of the QCM (Maxtek, Inc. P/N 124200-4) should be thermally insulated because ambient temperature changes will induce apparent mass changes. Air flow from room heating, ventilation, and air-conditioning (HVAC) should also be directed away from the ALD reactor, the reactor forelines, and the temperature monitoring system. Noise in the temperature monitoring system can be improved using battery-powered preamplifiers, stationary and moving signal averaging, and removal of ground loops. Using a thermally conductive gas (e.g., He instead of N_2) to purge the back of the QCM sensor also reduces the magnitude of the temperature-induced instantaneous mass transients. The higher thermal conductivity improves heat transfer between the QCM sensor and the QCM housing.

If all of the above-mentioned factors are considered, then reliable QCM measurements can be performed with minimal temperature-induced apparent mass changes. However, other sources of QCM mass error exist in addition to errors caused by temperature perturbation. These sources include the unknown active QCM surface area, surface roughness, changes in acoustic impedance for heavily loaded crystals,[31,32] and quartz crystal mode-hoping. These other sources of error are beyond the scope of this paper.

CONCLUSIONS

Temperature-induced apparent mass changes can significantly affect QCM measurements of ALD. The QCM is a very sensitive probe of both mass and temperature. Without knowing about the temperature-induced apparent mass changes, QCM transients corresponding to reactant exposures and ALD surface chemistry can be misinterpreted as resulting from adsorption/desorption processes. The cumulative effect of these temperature-induced apparent mass changes can also lead to errors in ALD growth rates.

The temperature-induced apparent mass changes are linked to the temperature profile of the ALD reactor. Colder temperatures prior to the QCM lead to positive mass transients. Hotter temperatures prior to the QCM lead to negative mass transients. Inert or other unreactive probe gases, such as SF_6, can be employed to optimize the temperature profile to minimize the temperature-induced apparent mass changes. In addition, adiabatic expansion of probe or reactant gases during gas admittance can seriously complicate these temperature effects.

When the temperature profile is optimized to minimize temperature-induced apparent mass changes, the QCM can monitor nearly ideal Al_2O_3 ALD that behaves according to expectations from the Al_2O_3 ALD surface chemistry. Probe gas pulses performed concurrently with the Al_2O_3 ALD confirm the negligible temperature-induced mass changes. The QCM is a valuable in situ probe of ALD. However, the QCM mass transients must be interpreted with care after minimizing the temperature-induced apparent mass changes.

ACKNOWLEDGMENT

The authors thank Applied Materials for primary funding of this work. Additional support was provided by the Air Force Office of Scientific Research. The authors also acknowledge Jeff Elam for his help and suggestion during the course of the project.

Received for review April 7, 2003. Accepted June 26, 2003.

AC030141U

(31) Benes, E. *J. Appl. Phys.* **1984**, *56*, 608.
(32) Wajid, A. *Rev. Sci. Instrum.* **1991**, *62*, 2026.